Analytical Optimal Solution of Perimeter Traffic Flow Control Based on MFD Dynamics: A Pontryagin's Maximum Principle Approach

Ali Aalipour, Hamed Kebriaei, *Senior Member, IEEE*, and Mohsen Ramezani, *Member, IEEE*

***Abstract*— Perimeter traffic flow control, based on the macroscopic fundamental diagram (MFD), has been introduced for traffic control and congestion management in large-scale networks. The perimeter controller is a set of traffic signals on the border between the regions manipulating the transfer flows with the aim to maximize the number of trips that reach their destinations. This paper tackles the optimal perimeter control of MFD systems for two-region urban networks which model heterogeneously congested cities. The modeling of the system results in nonlinear state dynamics, a non-quadratic cost function, and constraints on control actions and traffic states. We prove the existence of the optimal controller, analytically derive the optimal control policy, and introduce a numerical method to solve the optimal control policy. Based on the indirect optimal approach, HJB equation, and Pontryagin's maximum principal, we demonstrate that the optimal controller is in the form of Bang–Bang control. We apply the Chebyshev pseudospectral method to solve the two-point boundary value problem (TPBVP) for the proposed constrained optimal control problem. Consequently, the TPBVP is reduced to determination of the solution of a nonlinear system with algebraic equations. A numerical study is performed to measure the effectiveness of the proposed method.**

***Index Terms*— Large-scale urban networks, gating, network fundamental diagram, indirect optimal approach (IOA).**

I. Introduction

GROWING cities and unprecedented trend of urbanization have resulted in excessive traffic congestion that entails devising holistic congestion management techniques to ameliorate transportation systems performance. Transportation networks are inherently complex to analyze and control because of intricate dynamics of human decision making, convolved interactions between individuals at the network scale, and the spatial and temporal variations in the traffic supply and demand characteristics. Specifically, modeling the dynamics of traffic flow in urban environments with closely-spaced intersections is not a trivial task due to the unpredictability and immeasurability of micro-level traffic states. Hence, parsimonious models of traffic flow in large-scale urban networks are promising for developing traffic congestion control strategies to reduce aggravation of traffic jams.

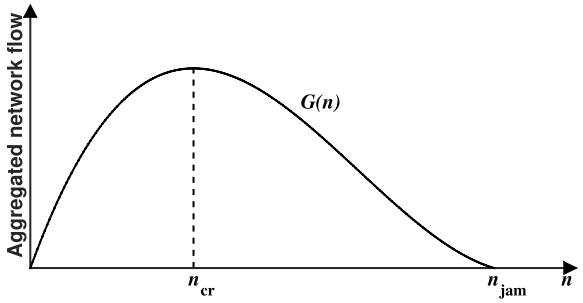

Fig. 1. A schematic of a unimodal and low-scatter MFD. $G(n)$ is the network outflow [veh/sec] that is a function of network vehicle accumulation n [veh].

Network Macroscopic Fundamental Diagram (MFD) is a parsimonious traffic model that relates network vehicle accumulation, n [veh], and aggregated network traffic outflow [veh/sec], see Fig. 1. Geroliminis and Daganzo [1] demonstrated the existence of such MFD relationship based on field data of a part of Yokohama, Japan. There are several studies on deriving the theoretical (MFD) functional relation between network-wide traffic states [2]–[5]. Moreover, the effect of congestion heterogeneity [6]–[8] and traffic assignment [9], [10] on the properties of MFD has been investigated. To address the effect of spatial pockets of congestion on properties of MFD, a clustering technique is developed in [11] to partition heterogeneous networks to homogeneous regions considering directional traffic flows on links. In this paper, similar to [12], we assume a heterogeneous urban network which can be partitioned into two regions with well-defined MFDs and the *analytical optimal* perimeter traffic control of the two-region MFD model is established.

Manuscript received August 23, 2017; revised March 1, 2018 and July 24, 2018; accepted September 23, 2018. Date of publication October 18, 2018; date of current version August 27, 2019. This work was supported by the Institute for Research in Fundamental Sciences (IPM) under Grant CS 1397-4-56. The Associate Editor for this paper was L. Li. *(Corresponding author: Hamed Kebriaei.)*

A. Aalipour is with the School of Electrical and Computer Engineering, College of Engineering, University of Tehran, Tehran 1417466191, Iran (e-mail: ali.aalipour@ut.ac.ir).

H. Kebriaei is with the School of Electrical and Computer Engineering, College of Engineering, University of Tehran, Tehran 1417466191 , Iran, and also with the School of Computer Science, Institute for Research in Fundamental Sciences (IPM), Tehran 1953833511, Iran (e-mail: kebriaei@ut.ac.ir).

M. Ramezani is with the School of Civil Engineering, The University of Sydney, Camperdown NSW 2006, Australia (e-mail: mohsen.ramezani@sydney.edu.au).

Digital Object Identifier 10.1109/TITS.2018.2873104

The MFD has been used in several studies as the traffic flow model to devise network-wide traffic control schemes. E.g. perimeter control in [12]–[15], region-based routing in [16], pricing in [17], design of transit systems in [18], and taxi dispatching in [19]. Moreover, [20]–[22] have implemented a classical feedback control method for traffic control based on the MFD concept. Furthermore, a robust perimeter controller with MFDs uncertainties based on a linearized system is introduced in [23] and [24] that employ Quantitative Feedback Theory (QFT) and interpolating-based approach, respectively. This paper follows a similar MFD-based modeling approach in formulation of the optimal perimeter control problem. The related literature explores sub-optimal solutions whereas this paper contributions are proving the existence of the optimal policy, deriving the closed-form optimal policy, and solving the optimal control numerically.

MFD estimation methods has been investigated in [25]–[28]. Recently, explicit modeling of boundary queues and their effects on perimeter control policies at two-region cities has been studied in [29]. Also, coupled and decoupled optimal perimeter control in cities with one-region and the explicit formulations of the optimal feedback control policies has been investigated in [30]. This paper tackles the analytical derivation of the optimal perimeter control of two-region urban cities formulated based on MFD. The Indirect Optimal Approach (IOA) based on Pontryagin's Maximum Principle (PMP) framework, is used to obtain the optimal control solution. We show that the optimal control is in the form of Bang-Bang. For further derivations of PMP in optimal control the reader can refer to [31]. The PMP has been studied for traffic control problems, e.g. [32], to derive the optimal signal settings of isolated signalized intersections. In this paper, the PMP is implemented for the perimeter control problem. It is worth to note that the optimal perimeter control of the two-region system is generalizable to systems with multiple regions. Consequently, the optimal perimeter control of multiple-region systems with MFD dynamics is in the form of Bang-Bang.

There are three steps required to implement indirect methods and derive the solution to the optimal problem: (i) forming the Hamiltonian, (ii) deriving the necessary conditions, and (iii) solving the boundary value problem using numerical methods. Note that the indirect methods benefit from a higher accuracy compared to the direct methods since the necessary conditions of optimality are satisfied by the solution. Pseudospectral methods are effective tools to solve the Two-Point Boundary Value Problem (TPBVP) and ordinary or partial differential equations with a high precision [33]–[35]. In this paper, the optimal perimeter control for two-region urban cities results in a nonlinear TPBVP, that is solved by a numerical method based on PMP and Chebyshev pseudospectral method.

The remainder of the paper is organized as follows. In Section II, the problem formulation for the two-region MFD system is introduced. The optimal control solution is obtained by applying the PMP approach in Section III. Section IV presents a numerical method for solving the TRBVP based on Pseudospectral method. We present results of the numerical case study examples in Section V and compare them with results of Model predictive Control (MPC) and Greedy Control approaches. Finally, The paper is concluded in Section VI.

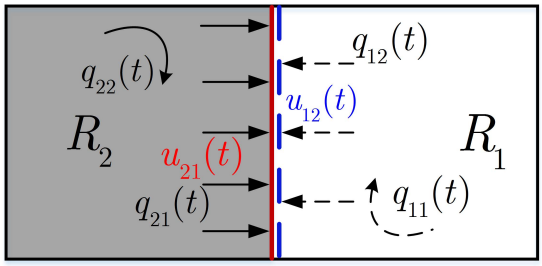

Fig. 2. Two-region MFDs system with two regions R_1 and R_2. $q_{11}(t)$, $q_{12}(t)$, $q_{21}(t)$, and $q_{22}(t)$ are four exogenous traffic demands and $u_{12}(t)$ and $u_{21}(t)$ are two perimeter controllers.

II. Two-Region MFD Model

The urban traffic model is described in this section where it is assumed that the urban network is divided into two regions. These two regions are modeled with a low-scatter MFD. Let us denote traffic states, n_{ij}, the number of vehicles categorized based on their current region i and their destination region j. This results in four traffic states, i.e. $n_{11}(t)$, $n_{12}(t)$, $n_{21}(t)$, and $n_{22}(t)$. The MFD is represented by $G_i(n_i(t))$, which is the trip completion flow in region i while $n_i(t)$ denotes the total accumulation of vehicles in region i at time t. Therefore, dynamics of the traffic states are as follows:

$$\dot{n}_{11}(t) = q_{11}(t) + u_{21}(t)M_{21}(t) - M_{11}(t) \tag{1a}$$
$$\dot{n}_{12}(t) = q_{12}(t) - u_{12}(t)M_{12}(t) \tag{1b}$$
$$\dot{n}_{21}(t) = q_{21}(t) - u_{21}(t)M_{21}(t) \tag{1c}$$
$$\dot{n}_{22}(t) = q_{22}(t) + u_{12}(t)M_{12}(t) - M_{22}(t), \tag{1d}$$

where $q_{ij}(t)$, $i, j = 1, 2$ is the exogenous demand of vehicles from region i to region j, and $n_i(t)$, $i = 1, 2$ is the total number of vehicles in region i. Evidently, $n_i(t) = \sum_j n_{ij}(t)$. The region i trip completion flow, $G_i(n_i(t))$, is the sum of both the internal and external trip completions respectively, $M_{ii}(t)$ and $M_{ij}(t)$. The internal and external trip completion flows are modeled based on the proportion between accumulations as $M_{ii}(t) = n_{ii}(t)/n_i(t) \cdot G_i(n_i(t))$ and $M_{ij}(t) = n_{ij}(t)/n_i(t) \cdot G_i(n_i(t))$. The schematic of a traffic network with two regions is depicted in Fig. 2.

Empirical and simulation findings, e.g. [1] and [12], demonstrate that the shape of MFD can be approximated by a third-order function of $n_i(t)$, i.e. $G_i(n_i(t)) = a_i \hat{\mathrm{A}} \cdot n_i(t)^3 + b_i \hat{\mathrm{A}} \cdot n_i(t)^2 + c_i \hat{\mathrm{A}} \cdot n_i(t)$, where a_i, b_i, and c_i are estimated parameters. Note that $n_i(t)$ lies within the range 0 to $n_{i,\mathrm{jam}}$, where $n_{i,\mathrm{jam}}$ denotes the accumulation at jammed traffic state of region i. This function is a non-symmetric unimodal curve skewed to the right, i.e. critical density that maximizes network flow is less than half of the jammed density, see Fig. 1.

The perimeter controllers are denoted by $u_{12}(t)$ and $u_{21}(t)$. The perimeter controllers can be realized and implemented by a set of traffic signals that are located on the border between the two regions manipulating the transfer flows between the

two regions. Hence, values of both $u_{12}(t)$ and $u_{21}(t)$ lie within the range 0 to 1. In practice, $u_{12}(t)$ and $u_{21}(t)$ might (i) need to satisfy certain constraints that may lead to a tighter bound than [0-1] and (ii) be dependent based on network topology, intersection design, and signal timing. In this paper, we assume $u_{12}(t)$ and $u_{21}(t)$ are independent. Note that only the inter-region transfer flows, $M_{ij}(t)$, are controllable by the perimeter controllers, contrary to the internal outflows $M_{ii}(t)$. Moreover, it is assumed in (1) that vehicles pass the border between the two regions only one time and the shape of the MFDs will not be affected by the perimeter control. In the next section, we demonstrate the analytical derivation of the optimal perimeter control for system (1).

III. Optimal Perimeter Control Problem

In this section, a criterion is defined such that the number of vehicles that arrive at their destination are maximized. Thus, formulation of the optimal control problem for the two-region MFD is as below:

$$J = \max_{u_{12}(t),u_{21}(t)} \int_{t_0}^{t_f} (M_{11}(t) + M_{22}(t))\,\mathrm{d}t = \min_{u_{12}(t),u_{21}(t)} \int_{t_0}^{t_f} -(M_{11}(t) + M_{22}(t))\,\mathrm{d}t, \tag{2}$$

subject to nonlinear dynamic equations (1), and

$$n_{11}(t) + n_{12}(t) \le n_{1,\mathrm{jam}}, \tag{3}$$

$$n_{21}(t) + n_{22}(t) \le n_{2,\mathrm{jam}}, \tag{4}$$

$$0 \le u_{\min} \le u_{12}(t) \le u_{\max} \le 1, \tag{5}$$

$$0 \le u_{\min} \le u_{21}(t) \le u_{\max} \le 1, \tag{6}$$

$$n_{11}(t_0) = n_{11,0}; \quad n_{12}(t_0) = n_{12,0}; \quad n_{21}(t_0) = n_{21,0}; \quad n_{22}(t_0) = n_{22,0}, \tag{7}$$

where time t_f is fixed and the final states, i.e. $n_{11}(t_f)$, $n_{12}(t_f)$, $n_{21}(t_f)$, and $n_{22}(t_f)$, are free. The initial accumulations at t_0 are $n_{ij,0}$, $i, j = 1, 2$. Accumulations at the jammed density are $n_{1,\mathrm{jam}}$ and $n_{2,\mathrm{jam}}$ [veh] for regions 1 and 2, respectively. Constraints (3) and (4) represent the upper bound of region accumulation. In Appendix A, we show that states of system (1) are greater than or equal to zero, i.e. $0 \le n_{ij}(t)$, with positive initial accumulations and positive exogenous demands. The lower and upper bounds of $u_{12}(t)$ and $u_{21}(t)$ are defined as $u_{\min}$ and $u_{\max}$, respectively. Note that without loss of generality, we assume $u_{\min}$ and $u_{\max}$ are unique for both u_{12} and u_{21}. This assumption can be readily relaxed.

The optimal control problem (1)-(7) is associated with a nonlinear non-quadratic cost function and nonlinear state dynamics, and inequality state and control constraints. To proceed with the derivation of the optimal solution, we reformulate the state constraints (3) and (4) according to the state inequality constraints given in (40) in Appendix B. Hence, an extra state variable, i.e. $n_e(t)$, is formed based on (41) with initial condition equal to zero. For the sake of brevity, we define $\mathbf{x}^T = (x_1(t), \cdots, x_5(t)) = (n_{11}(t), n_{12}(t), n_{21}(t), n_{22}(t), n_e(t))$.

We obtain the optimal perimeter control problem solution by applying the PMP based on procedure proposed in [31] and [36]. Interested reader can further refer to [37]–[39] for other methods to address states constraint in optimal control problems. To find the solution of the optimal problem by the IOA, at first, the Hamiltonian should be formed. State, i.e. **x**, and co-state, i.e. **p**, dynamic equations are then obtained by the Hamiltonian. Afterward, the optimal perimeter control problem can be solved. Formulating the Hamiltonian is as follows:

$$\begin{aligned} H(x,u,p,t) &= -M_{11}(t) - M_{22}(t) + \mathbf{p}^T(t)\cdot[\mathbf{f}(\mathbf{x}(t),\mathbf{u}(t),\mathbf{q}(t)), \dot{n}_e(t)] \\ &= -M_{11}(t) - M_{22}(t) \\ &\quad + p_1(t)\cdot\big(q_{11}(t) + u_{21}(t)M_{21}(t) - M_{11}(t)\big) \\ &\quad + p_2(t)\cdot\big(q_{12}(t) - u_{12}(t)M_{12}(t)\big) \\ &\quad + p_3(t)\cdot\big(q_{21}(t) - u_{21}(t)M_{21}(t)\big) \\ &\quad + p_4(t)\cdot\big(q_{22}(t) + u_{12}(t)M_{12}(t) - M_{22}(t)\big) \\ &\quad + p_5(t)\cdot\big((n_{1,\mathrm{jam}} - x_1(t) - x_2(t))^2 \\ &\quad \times \mathcal{U}(-(n_{1,\mathrm{jam}} - x_1(t) - x_2(t))) \\ &\quad + (n_{2,\mathrm{jam}} - x_3(t) - x_4(t))^2\mathcal{U}(-(n_{2,\mathrm{jam}} - x_3(t) - x_4(t)))\big), \end{aligned} \tag{8}$$

where $\mathbf{f}(\mathbf{x}(t), \mathbf{u}(t), \mathbf{q}(t))$ is the compressed form of (1), $\mathbf{p} = [p_1(t), ..., p_5(t)]$ is the co-states vector, $\mathbf{q}(t) = [q_{11}(t), q_{12}(t), q_{21}(t), q_{22}(t)]^{\mathrm{T}}$ is the vector representation of the traffic demands, $\mathbf{u}(t) = [u_{12}(t), u_{21}(t)]^{\mathrm{T}}$ is controller vector, and $\mathcal{U}(.)$ is a unit Heaviside step function that is defined in (42).

In the second step, the necessary optimality conditions for the states are obtained by $\dot{x}^* = \frac{\partial H}{\partial p}$. As a result, we can write these conditions as follows:

$$\dot{x}_1^*(t) = q_{11}(t) + u_{21}^*(t)M_{21}^*(t) - M_{11}^*(t) \tag{9a}$$

$$\dot{x}_2^*(t) = q_{12}(t) - u_{12}^*(t)M_{12}^*(t) \tag{9b}$$

$$\dot{x}_3^*(t) = q_{21}(t) - u_{21}^*(t)M_{21}^*(t) \tag{9c}$$

$$\dot{x}_4^*(t) = q_{22}(t) + u_{12}^*(t)M_{12}^*(t) - M_{22}^*(t) \tag{9d}$$

$$\begin{aligned} \dot{x}_5^*(t) &= (x_1^*(t) + x_2^*(t) - n_{1,\mathrm{jam}})^2 \\ &\quad \times \mathcal{U}(-(n_{1,\mathrm{jam}} - x_1^*(t) - x_2^*(t))) \\ &\quad + (x_3^*(t) + x_4^*(t) - n_{2,\mathrm{jam}})^2 \\ &\quad \times \mathcal{U}(-(n_{2,\mathrm{jam}} - x_3^*(t) - x_4^*(t))). \end{aligned} \tag{9e}$$

In a similar manner, the required optimality conditions for the co-states are derived by $\dot{p}^* = -\frac{\partial H}{\partial x}$. Therefore, we have

$$\begin{aligned} \dot{p}_1^*(t) &= (1 + p_1^*(t))\cdot\frac{\partial M_{11}}{\partial x_1} + (p_2^*(t) - p_4^*(t))\cdot u_{12}^*(t)\cdot\frac{\partial M_{12}}{\partial x_1} \\ &\quad - 2\times p_5^*(t)\cdot[(x_1^*(t) + x_2^*(t) - n_{1,\mathrm{jam}}) \\ &\quad \times \mathcal{U}(-(n_{1,\mathrm{jam}} - x_1^*(t) - x_2^*(t)))] \end{aligned} \tag{10a}$$

$$\begin{aligned} \dot{p}_2^*(t) &= (1 + p_1^*(t))\cdot\frac{\partial M_{11}}{\partial x_2} + (p_2^*(t) - p_4^*(t))\cdot u_{12}^*(t)\cdot\frac{\partial M_{12}}{\partial x_2} \\ &\quad - 2\times p_5^*(t)\cdot[(x_1^*(t) + x_2^*(t) - n_{1,\mathrm{jam}}) \\ &\quad \times \mathcal{U}(-(n_{1,\mathrm{jam}} - x_1^*(t) - x_2^*(t)))] \end{aligned} \tag{10b}$$

$$\begin{aligned} \dot{p}_3^*(t) &= (1 + p_4^*(t))\cdot\frac{\partial M_{22}}{\partial x_3} + (p_3^*(t) - p_1^*(t))\cdot u_{21}^*(t)\cdot\frac{\partial M_{21}}{\partial x_3} \\ &\quad - 2\times p_5^*(t)\cdot[(x_3^*(t) + x_4^*(t) - n_{2,\mathrm{jam}}) \\ &\quad \times \mathcal{U}(-(n_{2,\mathrm{jam}} - x_3^*(t) - x_4^*(t)))] \end{aligned} \tag{10c}$$

$$\dot{p}_4^*(t) = (1 + p_4^*(t)) \cdot \frac{\partial M_{22}}{\partial x_4} + (p_3^*(t) - p_1^*(t)) \cdot u_{21}^*(t) \cdot \frac{\partial M_{21}}{\partial x_4} - 2 \times p_5^*(t) \cdot [(x_3^*(t) + x_4^*(t) - n_{2,\text{jam}}) \times \mathcal{U}(-(n_{2,\text{jam}} - x_3^*(t) - x_4^*(t)))] \quad (10d)$$

$$\dot{p}_5^*(t) = 0. \quad (10e)$$

Note that the terminal conditions for co-states (10), i.e. $(p_1(t_\text{f}), \ldots, p_4(t_\text{f}))$, are zero because there is no terminal cost in objective function (2). In the third step, existence of the solution to the optimal perimeter control problem is discussed. In the above equations, $\dot{p}_5^*(t)$ is zero because Hamiltonian (8) does not include $x_5(t)$. That is $p_5^*(t)$ is a constant. It is evident in Equation (9e) that $\dot{x}_5^*(t) \geq 0$. We further set the initial condition of this state as $x_5^*(t_0) = 0$, see Equation (16). Therefore, if the terminal condition is obtained as $x_5^*(t_\text{f}) = 0$, then $\dot{x}_5^*$ should be zero during interval $t \in [t_0\, t_\text{f}]$. Accordingly, the state constraints (3) and (4) are satisfied in $t \in [t_0\, t_\text{f}]$ if and only if $\dot{x}_5^* = 0$ for $t \in [t_0\, t_\text{f}]$.

To implement this, the constant value of p_5 (i.e. the corresponding co-state of x_5^*) needs to be determined in order to ensure $x_5^*(t_\text{f}) = 0$. The procedure of finding an appropriate constant value for p_5 can be done by an iterative algorithm or a search method. It is worth to mention that the proposed approach (defining new state variable x_5^* and finding p_5 such that $x_5^*(t_\text{f}) = 0$) provides a sufficient but not necessary condition to satisfy constraints (3) and (4). Nevertheless, in the following Proposition we show that under a certain condition there exist an optimal control solution and the optimal controller is in the form of Bang-Bang.

Proposition 1: If there exist a feasible set of control inputs for system (1) *to satisfy* (3)-(6)*, then the optimal perimeter control for two-region system* (1)-(7) *exists and is in the form of Bang-Bang.*

Proof: The integrand in (2) is continuous and locally Lipschitz. Due to constraints (3) and (4) on the states and Appendix A, the integrand in (2) is finite and bounded. In addition, given constraints (3) and (4) and bounds on perimeter controllers, Hamiltonian (8) can be minimized. Hence, optimal controllers exist and can be obtained. By omitting the terms not related to control inputs, i.e. $u_{12}(t)$ and $u_{21}(t)$, we can express the Hamiltonian as:

$$H^* = u_{12}(t) M_{12}(t) (p_4(t) - p_2(t)) + u_{21}(t) M_{21}(t) (p_1(t) - p_3(t)). \quad (11)$$

Due to the linear relationship between H and the perimeter controllers $u_{12}(t)$ and $u_{21}(t)$ (and $M_{12}(t)$ and $M_{21}(t)$ being positive), the optimal controllers are

$$u_{12}^*(t) = \frac{u_\text{max} + u_\text{min}}{2} + \frac{u_\text{max} - u_\text{min}}{2} \cdot \text{sgn}\big(p_2(t) - p_4(t)\big), \quad (12)$$

$$u_{21}^*(t) = \frac{u_\text{max} + u_\text{min}}{2} + \frac{u_\text{max} - u_\text{min}}{2} \cdot \text{sgn}\big(p_3(t) - p_1(t)\big). \quad (13)$$

■

Remark 1: The result of Proposition 1 can be extended to a generalized multiple R-region system following the same modeling approach in (1) *and similar constraint optimal control problem in* (2)-(7)*. The optimal perimeter controllers are in form of Bang-Bang.*

Objective function (2) includes no measures of perimeter controllers. In addition, perimeter controllers are bounded, see (5) and (6). For these reasons, optimal controllers are obtained in the form of Bang-Bang. Note that, Proposition 1 is consistent with [40] where a similar conclusion is derived for a single region MFD system. Equation (12) demonstrates that based on relative difference between p_2 and p_4 (which are time-varying) optimal perimeter controller $u_{12}^*(t)$ might be either u_max or u_min. In the same manner, relative difference between p_1 and p_3 in (13) determines optimal perimeter controller $u_{21}^*(t)$ might be either u_max or u_min. Thus, to obtain optimal perimeter controllers (12) and (13), co-states are needed. Having initial values of states and final values of co-states, leads us to a TPBVP that is extremely difficult to solve analytically. Hence, numerical methods are needed to solve the TPBVP, which is introduced in the next section.

IV. Numerical Method for Solving Two-Point Boundary Value Problems

Solving the constrained optimal control problem, requires the solution to a TPBVP in which initial conditions of the states of the system, i.e. $n_{ij,0}$, and the terminal conditions of the co-states, i.e. $(p_1(t_\text{f}), \ldots, p_4(t_\text{f}))$, are known (equal to zero). To solve a TPBVP of ordinary differential equations (ODE) similar to (9) and (10), shooting methods are well-studied techniques [41]. However, if a small change occurs in the initial conditions, a significant change can appear in the terminal conditions. This is the main drawback of shooting methods. In addition, a precise estimation of the Jacobian matrix in Newton iterations is needed, which is numerically expensive to obtain because of nonlinearity of the ODEs.

In this section, briefly, the main properties and elements of *Chebyshev pseudospectral approach*, which has been recently proposed and developed in [42], are presented. By implementing Chebyshev pseudospectral method, TPBVP ODE in (9) and (10) is reduced to a set of algebraic equations. The main reason of using Chebyshev polynomials as the basis functions is that the partial sums of a Chebyshev approximation of a continuous function converge faster in comparison with other orthogonal polynomials like Legendre, see [33]. Description of Chebyshev pseudospectral method is given in Appendix C. For further information, the reader is referred to [33], [43], and [44].

Assume nonlinear system (1) and objective function (2) are associated with a fixed final time t_f. After minimizing Hamiltonian (8) with respect to the states and co-states and substituting the optimal controllers (12) and (13) in the differential equations (9) and (10), we obtain

$$\dot{\mathbf{x}}(t) = \mathbf{h}(t, \mathbf{x}(t), \mathbf{p}(t)), \quad (14)$$

$$\dot{\mathbf{p}}(t) = \mathbf{g}(t, \mathbf{x}(t), \mathbf{p}(t)), \quad (15)$$

where $\mathbf{h}$ and $\mathbf{g}$ are nonlinear vector functions of (9) and (10), respectively, with the boundary conditions as

$$\mathbf{x}(0) = (n_{11,0}, n_{12,0}, n_{21,0}, n_{22,0}, 0) = x_{j0}, \quad j = 1, ..., 5, \quad (16)$$

$$\mathbf{p}(t_{\mathrm{f}}) = (0,0,0,0,c) = p_{jN}, \quad j = 1, ..., 5 \tag{17}$$

where c is a constant.

Proposition 2: Implementing Chebyshev pseudospectral method, a set of $10(N+1)$ *nonlinear algebraic equations*

$$\mathrm{RES}_{\mathbf{x}}(t) \triangleq \dot{\mathbf{x}}^N(t) - \mathbf{h}(t, \mathbf{x}^N(t), \mathbf{p}^N(t))$$

and

$$\mathrm{RES}_{\mathbf{p}}(t) \triangleq \dot{\mathbf{p}}^N(t) - \mathbf{g}(t, \mathbf{x}^N(t), \mathbf{p}^N(t))$$

are generated from (14) *and* (15)*, where N is the number of function approximators. With* $N \longrightarrow \infty$*, difference between Chebyshev approximation and the optimal solution converges to zero.*

Proof: Given t_0 and t_{f} are the two endpoints, roots of $\dot{T}_N^*(t)$ called *shifted Chebyshev-Gauss-Lobatto nodes* are

$$t_l = \frac{(t_{\mathrm{f}} - t_0)}{2}\left(1 + \cos\left(\frac{(N-l)\pi}{N}\right)\right), \quad l = 0, ..., N. \tag{18}$$

Using the following approximations

$$x_j(t) \approx x_j^N(t) = (t - t_0)\sum_{k=0}^{N} X_{jk} T_k^*(t) + x_{j0}, \quad j = 1, ..., 5, \tag{19}$$

$$p_j(t) \approx p_j^N(t) = (t - t_N)\sum_{k=0}^{N} P_{jk} T_k^*(t) + p_{jN}, \quad j = 1, ..., 5, \tag{20}$$

yields

$$x_j^N(t_0) = x_{j0}, \quad j = 1, ..., 5, \tag{21}$$

$$p_j^N(t_N) = p_{jN} = (0,0,0,0,c), \tag{22}$$

where the approximation error uniformly decreases by increasing N [42]. Employing (19) and (20), the approximated first derivatives of $x_j(t)$ and $p_j(t)$ are

$$\begin{aligned}\dot{x}_j^N(t) &= \sum_{k=0}^{N} X_{jk} T_k^*(t) + \frac{2(t - t_0)}{(t_{\mathrm{f}} - t_0)}\sum_{k=0}^{N} X_{jk}^{(1)} T_k^*(t) \\ &= \sum_{k=0}^{N}\left[X_{jk} + \frac{2X_{jk}^{(1)}}{(t_{\mathrm{f}} - t_0)}(t - t_0)\right] T_k^*(t), \quad j = 1, ..., 5,\end{aligned} \tag{23}$$

$$\begin{aligned}\dot{p}_j^N(t) &= \sum_{k=0}^{N} P_{jk} T_k^*(t) + \frac{2(t - t_N)}{(t_{\mathrm{f}} - t_0)}\sum_{k=0}^{N} P_{jk}^{(1)} T_k^*(t) \\ &= \sum_{k=0}^{N}\left[P_{jk} + \frac{2P_{jk}^{(1)}}{(t_{\mathrm{f}} - t_0)}(t - t_N)\right] T_k^*(t), \quad j = 1, ..., 5.\end{aligned} \tag{24}$$

Using X_{jk} and P_{jk}, the coefficient $X_{jk}^{(1)}$ and $P_{jk}^{(1)}$ are given by

$$X_{jk}^{(1)} = \frac{2}{c_k}\sum_{\substack{s=k+1 \\ (s+k)\mathrm{odd}}}^{N} sX_{js}, \quad k = 0, ..., N-1, \quad X_{jN}^{(1)} = 0, \tag{25}$$

$$P_{jk}^{(1)} = \frac{2}{c_k}\sum_{\substack{s=k+1 \\ (s+k)\mathrm{odd}}}^{N} s(s^2 - k^2)P_{js}, \quad k = 0, ..., N-1, \quad P_{jN}^{(1)} = 0, \tag{26}$$

where $c_0 = 2$ and $c_k = 1$, $k \geq 1$. Now, implementing (18)-(26), the residual functions can be written as

$$\mathrm{RES}_{\mathbf{x}}(t) = \dot{\mathbf{x}}^N(t) - \mathbf{h}(t, \mathbf{x}^N(t), \mathbf{p}^N(t)), \tag{27}$$

$$\mathrm{RES}_{\mathbf{p}}(t) = \dot{\mathbf{p}}^N(t) - \mathbf{g}(t, \mathbf{x}^N(t), \mathbf{p}^N(t)), \tag{28}$$

where

$$\mathbf{x}^N(t) = (x_1^N, \ldots, x_5^N), \tag{29}$$

$$\mathbf{p}^N(t) = (p_1^N, \ldots, p_5^N). \tag{30}$$

Setting $\mathrm{RES}_{\mathbf{x}}(t)$ and $\mathrm{RES}_{\mathbf{p}}(t)$ to zero at collocation points $\{t_l\}_{l=0}^N$, a set of $10(N+1)$ nonlinear algebraic equations are generated as follows:

$$\mathrm{RES}_{\mathbf{x}}(t_l) = 0, \quad l = 0, 1, \ldots, N, \tag{31}$$

$$\mathrm{RES}_{\mathbf{p}}(t_l) = 0, \quad l = 0, 1, \ldots, N. \tag{32}$$

Finally, the coefficients X_{jk} and P_{jk}, $k = 0, \cdots, N$, are obtained by solving (31) and (32) using numerical methods. ■

V. Numerical Experiments

In this section, first two-region MFD Plant is presented followed by the introduction of another Bang-Bang controller for comparison purposes. Then, two case studies are demonstrated to examine the properties of the proposed IOA. The IOA controller is also compared with a controller based on Model Predictive Control (MPC) approach.

A. Two-Region MFD Plant (Process Model)

In this paper, two sources of uncertainty in the modeling dynamics are accommodated, (i) the MFD modeling error and (ii) measurement noise in the exogenous traffic demands. The MFDs with errors are indicated by $\tilde{G}_1$ and $\tilde{G}_2$ for regions 1 and 2, respectively. We assume the MFD uncertainty is uniformly associated with the accumulation as:

$$\varepsilon(n_i(t)) \sim U(-\alpha_i \cdot n_i(t), \alpha_i \cdot n_i(t)), \tag{33}$$

where α_i, $i = 1, 2$, is a constant parameter. Hence, plant MFDs, i.e. $\tilde{G}_1$ and $\tilde{G}_2$, are

$$\tilde{G}_i(n_i(t)) = G_i(n_i(t)) + \varepsilon(n_i(t)). \tag{34}$$

Exogenous demand noise indicates stochastic recurrent and non-recurrent within-day variations in demand. The demand with noise considering a Gaussian distribution for demand noise is

$$\tilde{q}_{ij}(t) = \max(q_{ij}(t) + \mathcal{N}(0, \sigma_{ij}^2), 0), \tag{35}$$

where $i, j = 1, 2$ and $\sigma_{ij}^2(\mathrm{veh}^2/\mathrm{sec}^2)$ is the variance of the demand $q_{ij}(t)$.

Let us denote $\tilde{\mathbf{q}}(t) = \left[\tilde{q}_{11}(t), \tilde{q}_{12}(t), \tilde{q}_{21}(t), \tilde{q}_{22}(t)\right]^{\mathrm{T}}$ as the vector representation of the noisy traffic demand. Substituting the MFDs with errors (34), along with the noisy demand (35)

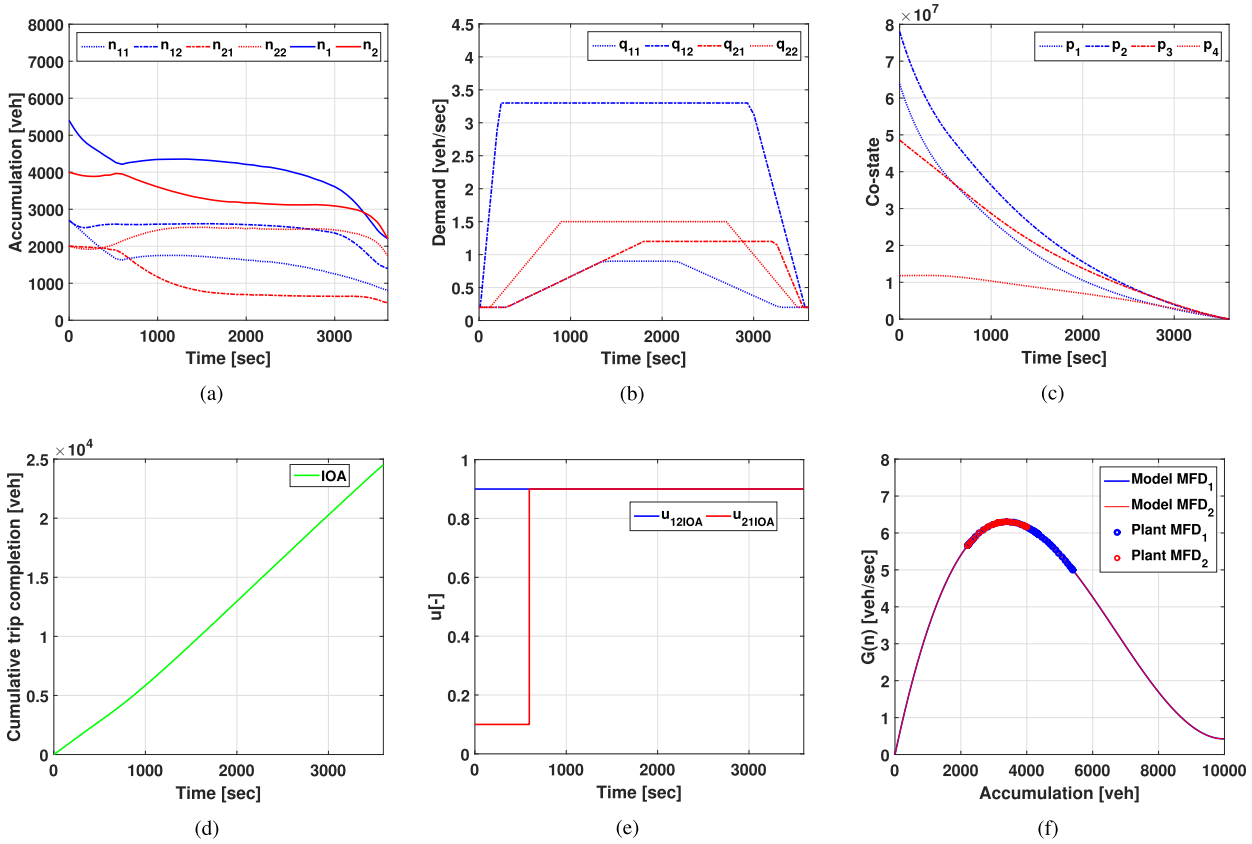

Fig. 3. Case study 1. Regions 1 and 2 are initially congested (without errors in MFDs and noise in demands): (a) Evolution of accumulations; (b) Demands; (c) Evolution of co-states; (d) Cumulative trip completion; (e) Perimeter controllers; (f) MFDs.

in dynamic equations (1), would results in compressed form of the two-region MFDs plant as fallows:

$$\frac{\mathrm{d}\tilde{\mathbf{n}}(t)}{\mathrm{d}t} = \mathbf{f}(\tilde{\mathbf{n}}(t), \mathbf{u}(t), \tilde{\mathbf{q}}(t), \boldsymbol{\varepsilon}(t)), \tag{36}$$

where $\boldsymbol{\varepsilon}(t) = \left[\varepsilon(\tilde{n}_i(t))\right]^{\mathrm{T}}$, $i = 1, 2$.

B. Greedy Control (GC)

To further investigate the performance of the IOA perimeter controller, comparisons are carried out with a Bang-Bang controller, namely Greedy Controller (GC). GC is a state feedback control specified through the current regional accumulations $n_1(t)$ and $n_2(t)$ and relative congestion level of each region to the critical accumulation, i.e. $n_{1,\mathrm{cr}}$ and $n_{2,\mathrm{cr}}$ [veh] where G_1 and G_2 are at maximum value, respectively. The GC control actions are listed in Table I.

TABLE I

GREEDY CONTROL ACTIONS, $u_{12}(t)$ AND $u_{21}(t)$

$[u_{12}(t), u_{21}(t)]$	$n_1(t) \le n_{1,\mathrm{cr}}$	$n_1(t) > n_{1,\mathrm{cr}}$
$n_2(t) \le n_{2,\mathrm{cr}}$	$[u_{\max}, u_{\max}]$	$[u_{\max}, u_{\min}]$
$n_2(t) > n_{2,\mathrm{cr}}$	$[u_{\min}, u_{\max}]$	$[u_{\max}, u_{\min}]$ if $\frac{n_1(t)}{n_{1,\mathrm{jam}}} > \frac{n_2(t)}{n_{2,\mathrm{jam}}}$ $[u_{\min}, u_{\max}]$ otherwise

C. Case Studies

Two case studies with time-varying traffic states are considered to evaluate the performance of the IOA. Comparisons are performed by applying the IOA, GC, MPC, and no controller (NC) to the nonlinear and noisy plant (36) with different levels of uncertainty. One case study is tested on the noisy plant where there are significant measurement errors on exogenous demands and MFD modeling. This is crucial to investigate the performance of the proposed optimal IOA where modeling mismatch is expected between a well-defined MFD and measured MFD.

Without loss of generality, we consider the well-defined MFDs for both regions are identical, where $G_i(n_i(t)) = (1.4877 \cdot 10^{-7} \cdot n_i^3 - 2.9815 \cdot 10^{-3} \cdot n_i^2 + 15.0912 \cdot n_i)/3600$, $i = 1, 2$; $n_{1,\mathrm{cr}} = n_{2,\mathrm{cr}} = 3400$ [veh]; $G_1(n_{1,\mathrm{cr}}) = G_2(n_{2,\mathrm{cr}}) = 6.31$ [veh/s]; and $n_{1,\mathrm{jam}} = n_{2,\mathrm{jam}} = 10000$ [veh]. This is in accordance with the MFD estimated in [1]. The lower and upper bounds of the perimeter controller are set to $u_{\min} = 0.1$ and $u_{\max} = 0.9$, respectively, to capture the policy restrictions on minimum and maximum green phase durations. The number of function approximators is set to $N = 60$ in all case studies. Moreover, the initial accumulations $n_1(t_0) = 5400$ and $n_2(t_0) = 4000$ are in congested regime (MFD part with the negative slope), where $n_2(t_0)$ is 18% higher than $n_{2,\mathrm{cr}}$ and $n_1(t_0)$ is 59% higher than $n_{1,\mathrm{cr}}$.

The results of Case study 1, which is associated with the IOA controller, with no noise in the demands and no errors

in the MFDs ($\alpha_1 = \alpha_2 = 0$) are depicted in Fig. 3. The time-varying demands are illustrated in Fig. 3(b), in which a peak hour with directional flows to Region 2 (i.e. the common destination of trips) is simulated. The evolution of accumulations $n_{ij}(t)$ and co-states over time are shown in Fig. 3(a) and Fig. 3(c), respectively. The cumulative trip completion, i.e. objective function (2), associated to the proposed IOA controller is depicted in Fig. 3(d). The control sequences $u_{12}(t)$ and $u_{21}(t)$ are depicted in Fig. 3(e) where the optimal perimeter controllers are in form of Bang-Bang. At $t = 600$ [sec], $u_{21}(t)$ switches from $u_{\min}$ to $u_{\max}$ that is associated with the event that the value of p_3 becomes greater than p_1. As illustrated in Fig. 3(f), MFDs $G_1(n_1(t))$ and $G_2(n_2(t))$ coincide, while the circle points are obtained based on (34) as $\tilde{G}_1$ and $\tilde{G}_2$. Note that in this case study, there are no errors in both MFDs.

Further to demonstrate the effectiveness of the proposed IOA controller, the same case study is tested with no controller (NC), GC, and MPC. Interested reader is refered to [12] for comprehensive description of MPC method. The evolution of accumulations corresponding to the NC, GC, and MPC are presented in Fig. 4(a), (c), and (e), respectively. With NC, both perimeter controllers are equal to $u_{\max}$ independent of traffic states, see Fig. 4(b). This scenario represents the lack of a network-scale type of traffic control scheme. The NC results in the gridlock of Region 1 (i.e. $n_1 = n_{1,\text{jam}}$) which happens at $t = 2280$ [sec]. (This is an example where the states of the system become unbounded and reach to n_{jam}).

Fig. 4(d) depicts the GC perimeter controller. Initially, GC assumes Region 1 as the region to be protected (from transfer flows from Region 2) by the perimeter controller because it is more congested than Region 2. Hence $u_{12} = u_{\max}$ and $u_{21} = u_{\min}$ until $t = 660$ [sec], when accumulation of Regions 1 and 2 become equal and afterwards the GC results in chattering perimeter control actions as the relative accumulation of regions toggle at each control step, which is set to 60 [sec]. This leads to simultaneous increase of accumulation in both regions, see Fig. 4(c). The MPC control actions follow a similar trend to IOA control actions. That is, u_{12} always equals to $u_{\max}$ and u_{21} starts from $u_{\min}$ increasing to $u_{\max}$, though for a long period of time u_{21} is between $u_{\min}$ and $u_{\max}$. MPC control actions are not in form of Bang-Bang and result in keeping the accumulation of Region 1 around 5000 [veh] and reducing Region 2 accumulation from 4000 [veh] to 3000 [veh].

The trip completions related to NC, GC, MPC, and IOA, for Case study 1 (error-free plant) are listed in Table II. The GC, MPC, and IOA controllers increase the total trip completion respectively by 26.4%, 74.3%, and 81.5% with respect to the No Control scenario. Evidently, the performance of MPC is less than of IOA because MPC is a sub-optimal control approach. It is worth to mention that the MPC requires a state feedback from the plant every control step (which is set to 60 [sec]), whereas IOA approach does not require a recurrent state feedback. This inherent structural feature of MPC helps to tackle modeling error. Case study 2 is devised to investigate the performance of IOA dealing with modeling error and demand prediction noise.

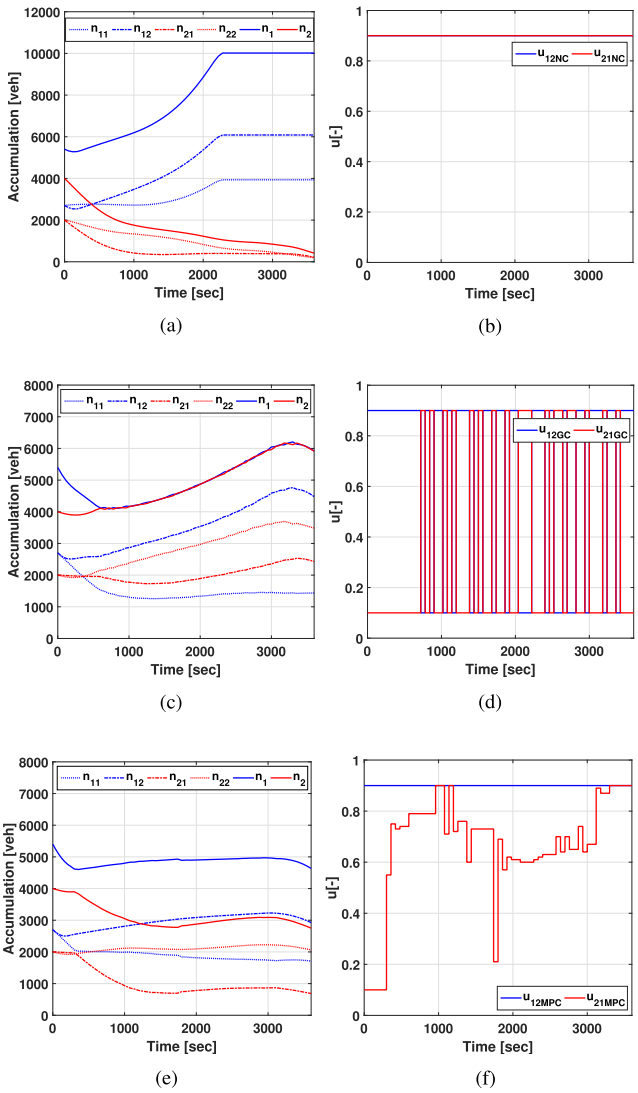

Fig. 4. Case study 1. Regions 1 and 2 are initially congested (with no error in MFDs and no noise in demands): (a) Evolution of accumulations with No Control; (b) Perimeter controllers when No Control is active ($u_{12}(t) = u_{21}(t) = u_{\max}$); (c) Evolution of GC accumulations; (d) GC perimeter controllers; (e) Evolution of MPC accumulations; (f) MPC perimeter controllers. Note that the range of accumulation axes are different.

Figure 5 illustrates the results of Case study 2 where the IOA controller is applied to the system similar to Case study 1 but with noise ($\sigma_{ij}^2 = 0.5$, $i, j = 1, 2$) in the demands (Fig. 5(b)) and errors ($\alpha_1 = \alpha_2 = 0.2$) in the MFDs (Fig. 5(c)). To derive the IOA, error-free MFD and noise-free demand are considered in formulations, hence the IOA controls of Case study 1 and 2 are similar though the system outputs are different.

Table II shows the trip completion of every controller for Case studies 1 and 2. Note that the results of Case study 2 are averaged over 20 runs to provide a more statistically accurate performance index. In both case studies, GC shows around 20-25% improvement compare to NC, whereas with noisy demands and errors in MFD the performance of MPC and IOA decreases. This is expected because modeling mismatch and error in prediction deteriorate the performance of model-based

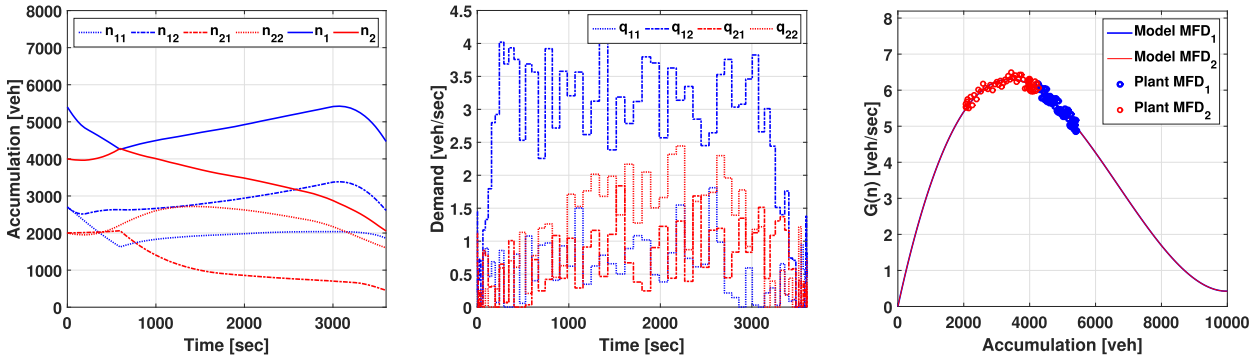

(a) (b) (c)

Fig. 5. Case study 2 with noise in demand and errors in MFDs: (a) Evolution of accumulations applying IOA; (b) Demands; (c) MFDs.

TABLE II

TOTAL TRIP COMPLETION [veh.10^3] FOR THE PROPOSED OPTIMAL IOA, MODEL PREDICTIVE CONTROLLER (MPC), GREEDY CONTROLLER (GC), AND NO CONTROL (NC). THE VALUES IN PARENTHESES INDICATE THE RELATIVE IMPROVEMENT OF GC, MPC, AND IOA WITH RESPECT TO THE NC PERFORMANCE. CASE STUDY 2 CONSIDERS MODELING ERROR AND MEASUREMENT NOISE

	$\alpha_1 = \alpha_2 = 0$, $\sigma_{ij}^2 = 0$, $i, j = 1, 2$			
Case study 1	NC	GC	MPC	IOA
	13.51	17.07 (26.4%)	23.55 (74.3%)	24.52 (81.5%)
	$\alpha_1 = \alpha_2 = 0.2$, $\sigma_{ij}^2 = 0.5$, $i, j = 1, 2$			
Case study 2	NC	GC	MPC	IOA
	13.64	16.33 (19.7%)	23.02 (68.8%)	23.23 (70.3%)

control approaches such as MPC and IOA. Nevertheless, MPC and IOA are still significantly more efficient than NC and GC. In Case study 2, IOA shows more than 1% improvement compare to MPC, which demonstrates that the proposed IOA is practical to tackle modeling mismatch. Note that MPC is more robust by design because of its rolling-horizon structure that requires recurrent state feedback to hinder the accumulation of error in states over time. Although decrease in MPC performance between Case studies 1 and 2 is less than of IOA, outcome of IOA is still higher than of MPC. It is expected that very high level of errors and noise deteriorate more the performance of IOA.

Numerical results of Case studies 1 and 2 demonstrate that the proposed IOA controller is effective, outperforms Bang-Bang GC, NC, and MPC and can tackle uncertainties in demand estimation and undesired patterns in aggregated MFD modeling such as hysteresis loops.

VI. CONCLUSION

In this paper, traffic flow dynamics of a heterogeneous large-scale urban network are modeled based on the MFD concept. A two-region MFD model was used to develop an optimal traffic control problem. The optimal perimeter control problem for two urban regions with nonlinear state dynamics, non-quadratic cost, and input and state constraints has been solved by applying the IOA scheme. Using HJB equation and Pontryagin's maximum principal, *we analytically prove that if a perimeter controller stabilizes the system then the optimal controller exists and is in the form of Bang-Bang*.

The optimal control actions depend on the definition of co-states that leads to a set of ordinary deferential equations for traffic states (i.e. accumulation of vehicles in each region based on the destination) and co-states. Obtaining the optimal control problem requires to solve the set of states and co-states ODEs where the initial conditions of (traffic) states and final conditions of the co-states are known. Hence, the constrained optimal control problem was solved numerically as a Two-Point Boundary Value Problem (TPBVP). Chebyshev pseudospectral method was implemented to solve the TPBVP for the proposed constrained optimal control. As a result, the TPBVP were reduced to solve a system with algebraic equations. Numerical case studies show the performance and properties of IOA.

Future work involves integration of robustness and optimality in the control methodology. This is a crucial step towards designing large-scale control strategies because modeling and measurement uncertainties are inevitable at the city level. Furthermore, the theoretical investigation on optimal control of multimodal MFDs (e.g. with public transport, taxis, etc.) is of great importance for devising holistic congestion management frameworks. This is a challenging future research direction.

APPENDIX A
POSITIVITY OF THE SYSTEM

Lemma 1: The set

$$\{0 \leq n_{11}(t), n_{12}(t), n_{21}(t), n_{22}(t)\}, \tag{37}$$

is an invariant set for system (1) *given* $0 \leq q_{ij}(t)$.

Proof: The Lemma states that if $0 \leq n_{ij,0}$ then $0 \leq n_{ij}(t)$. When $n_{ij}(t)$ becomes zero in system (1), the negative term at the RHS, i.e. $M_{ij}(t)$, becomes zero, hence the RHS will be positive or equal to zero. Thus, $\dot{n}_{ij}(t)$ will not be negative. So, states cannot be negative.

Intuitively, system (1) is a physical system where n represents the number of vehicles which cannot be a negative variable.

■

APPENDIX B
PENALTY FUNCTION METHOD FOR CONSTRAINED OPTIMAL PROBLEM

The following mathematical description is based on [31] pages 352-354. Consider system (38) and the performance index as (39).

$$\dot{\mathbf{x}}(t) = \mathbf{f}(\mathbf{x}(t), \mathbf{u}(t), t), \tag{38}$$

$$J = h(\mathbf{x}(t_{\mathrm{f}})) + \min_{\mathbf{u}(t)} \int_{t_0}^{t_{\mathbf{f}}} V(\mathbf{x}, \mathbf{u}(t), t)\mathrm{d}t, \tag{39}$$

where $\mathbf{x}(t)$ and $\mathbf{u}(t)$ are state and control vectors and n is dimension of the state vector. The constraints of the system are expressed as the following inequalities:

$$\begin{aligned} & g_1(x_1(t), ..., x_n(t), t) \geq 0 \\ & \vdots \\ & g_p(x_1(t), ..., x_n(t), t) \geq 0. \end{aligned} \tag{40}$$

A new variable $x_{n+1}(t)$ is defined by:

$$\begin{aligned} \dot{x}_{n+1}(t) &\triangleq f_{n+1}(\mathbf{x}(t), t) \\ &= [g_1(\mathbf{x}(t), t)]^2 \mathcal{U}\Big(-g_1(\mathbf{x}(t), t)\Big) \\ &\quad + \cdots + \big[g_p(\mathbf{x}(t), t)\big]^2 \mathcal{U}\Big(-g_p(\mathbf{x}(t), t)\Big), \end{aligned} \tag{41}$$

where $\mathcal{U}$ is a unit Heaviside step function defined as:

$$\mathcal{U}(-g_i) = \begin{cases} 0, & \text{if } g_i(\mathbf{x}(t), t) \geq 0 \\ 1, & \text{if } g_i(\mathbf{x}(t), t) < 0. \end{cases} \tag{42}$$

When any of the constraints (40) are violated, $\dot{x}_{n+1}(t)$ becomes positive, while in case of satisfaction of the constraints, $\dot{x}_{n+1}(t)$ equals zero.

APPENDIX C
CHEBYSHEV PSEUDOSPECTRAL METHOD

The following mathematical description is extracted from [33], [42], and [43].

The Chebyshev polynomials, $T_n(x)$, $n = 0, 1, 2, ...$, arise as the solution to the singular Sturm-Liouville problem

$$\left(1 - x^2\right) T_n''(x) - x T_n'(x) + n^2 T_n(x) = 0. \tag{43}$$

On the interval $[-1, 1]$, the Chebyshev polynomials are orthogonal with respect to L^2_ω inner projection, i.e.,

$$\int_{-1}^{1} \frac{T_n(x) T_m(x)}{\sqrt{1 - x^2}} \mathrm{d}x = \frac{\pi}{2} c_n \delta_{nm}, \tag{44}$$

where $\omega(x) = \frac{1}{\sqrt{1-x^2}}$ is the weight function, $c_0 = 2$, $c_n = 1$ for $n \geq 1$, and δ_{nm} is the Kroneker delta function. The Chebyshev polynomials can also be defined by the recurrence equation as follows:

$$T_{n+1}(x) = 2x T_n(x) - T_{n-1}(x), \quad n = 1, 2, \ldots, \tag{45}$$

where $T_0(x) = 1$ and $T_1(x) = x$.

Using Chebyshev polynomials, a function $f(x) \in L^2_\omega(-1, 1)$ can be represented as

$$f(x) = \sum_{j=0}^{\infty} f_j T_j(x), \tag{46}$$

where the coefficients f_j are acquired by

$$f_j = \frac{2}{\pi c_j} \int_{-1}^{1} \frac{f(x) T_j(x)}{\sqrt{1 - x^2}} \mathrm{d}x, \quad j = 0, 1, 2, \ldots. \tag{47}$$

To use the Chebyshev polynomials on interval $[0, T]$, we need to shift the defining domain. This is obtained by the following variable substitution

$$x = 2\left(\frac{t}{T}\right) - 1. \tag{48}$$

Denoting the shifted Chebyshev polynomials as $T^*_n \triangleq T_n\left(2\left(\frac{t}{T}\right) - 1\right)$, they are given by the following recurrence equation

$$T^*_{n+1}(t) = \left(4\left(\frac{t}{T}\right) - 2\right) T^*_n(t) - T^*_{n-1}(t), \quad n = 1, 2, \ldots, \tag{49}$$

where $T^*_0(t) = 1$ and $T^*_1(t) = \left(2\left(\frac{t}{T}\right) - 1\right)$. For the shifted Chebyshev polynomials, the orthogonally condition is written as

$$\int_0^T \frac{T^*_n(t) T^*_m(t)}{\sqrt{Tt - t^2}} \mathrm{d}t = \frac{\pi}{2} c_n \delta_{nm}. \tag{50}$$

Using shifted Chebyshev polynomials, any function $f(t) \in L^2_\omega(0, T)$ can be approximated in the form

$$f^N(t) \approx \sum_{j=0}^{N} f^*_j T^*_j(t), \tag{51}$$

where

$$f^*_j = \frac{2}{\pi c_j} \int_{-1}^{1} \frac{f\left(\left(\frac{T}{2}\right)(t+1)\right) T_j(t)}{\sqrt{1 - t^2}} \mathrm{d}t, \quad j = 0, \ldots, N. \tag{52}$$

We can also write the first derivative of $f^N(t)$ as

$$\dot{f}^N(t) \approx \frac{2}{T} \sum_{j=0}^{N} f^{(1)}_j T^*_j(t), \tag{53}$$

in which the coefficients $f^{(1)}_j$ are achieved using f_j

$$f^{(1)}_j = \frac{2}{c_j} \sum_{\substack{p=j+1 \\ (p+j)\,\mathrm{odd}}}^{N} p f^*_p, \quad j = 0, ..., N-1, \quad f^{(1)}_N = 0. \tag{54}$$

REFERENCES

[1] N. Geroliminis and C. F. Daganzo, "Existence of urban-scale macroscopic fundamental diagrams: Some experimental findings," *Transp. Res. B, Methodol.*, vol. 42, no. 9, pp. 759–770, Nov. 2008.

[2] C. F. Daganzo and N. Geroliminis, "An analytical approximation for the macroscopic fundamental diagram of urban traffic," *Transp. Res. B, Methodol.*, vol. 42, no. 9, pp. 771–781, Nov. 2008.

[3] N. Gerolimins and B. Boyaci, "The effect of variability of urban systems characteristics in the network capacity," *Transp. Res. B, Methodol.*, vol. 46, no. 10, pp. 1607–1623, 2012.

[4] C. F. Daganzo, V. V. Gayah, and E. J. Gonzales, "Macroscopic relations of urban traffic variables: Bifurcations, multivaluedness and instability," *Transp. Res. B, Methodol.*, vol. 45, no. 1, pp. 278–288, 2011.

[5] J. A. Laval and F. Castrillón, "Stochastic approximations for the macroscopic fundamental diagram of urban networks," *Transp. Res. B, Methodol.*, vol. 81, pp. 904–916, Nov. 2015.

[6] M. Ramezani, J. Haddad, and N. Geroliminis, "Dynamics of heterogeneity in urban networks: Aggregated traffic modeling and hierarchical control," *Transp. Res. B, Methodol.*, vol. 74, pp. 1–19, Apr. 2015.

[7] V. L. Knoop, H. van Lint, and S. P. Hoogendoorn, "Traffic dynamics: Its impact on the macroscopic fundamental diagram," *Phys. A, Stat. Mech. Appl.*, vol. 438, pp. 236–250, Nov. 2015.

[8] H. S. Mahmassani, M. Saberi, and A. Zockaie, "Urban network gridlock: Theory, characteristics, and dynamics," *Transp. Res. C, Emerg. Technol.*, vol. 36, pp. 480–497, Nov. 2013.

[9] M. Yildirimoglu and N. Geroliminis, "Approximating dynamic equilibrium conditions with macroscopic fundamental diagrams," *Transp. Res. B, Methodol.*, vol. 70, pp. 186–200, Dec. 2014.

[10] J. A. Laval, L. Leclercq, and N. Chiabaut, "Minimal parameter formulations of the dynamic user equilibrium using macroscopic urban models: Freeway vs city streets revisited," *Transp. Res. Procedia*, vol. 23, pp. 517–530, Jan. 2017.

[11] M. Saeedmanesh and N. Geroliminis, "Clustering of heterogeneous networks with directional flows based on 'Snake' similarities," *Transp. Res. B, Methodol.*, vol. 91, pp. 250–269, Sep. 2016.

[12] N. Geroliminis, J. Haddad, and M. Ramezani, "Optimal perimeter control for two urban regions with macroscopic fundamental diagrams: A model predictive approach," *IEEE Trans. Intell. Transp. Syst.*, vol. 14, no. 1, pp. 348–359, Mar. 2013.

[13] K. Yang, N. Zheng, and M. Menendez, "Multi-scale perimeter control approach in a connected-vehicle environment," *Transp. Res. C, Emerg. Technol.*, vol. 94, pp. 32–49, Sep. 2018.

[14] A. Aalipour, H. Kebriaei, and M. Ramezani, "Nonlinear robust traffic flow control in urban networks," *IFAC-PapersOnLine*, vol. 50, no. 1, pp. 8537–8542, 2017.

[15] A. Kouvelas, M. Saeedmanesh, and N. Geroliminis, "Enhancing model-based feedback perimeter control with data-driven online adaptive optimization," *Transp. Res. B, Methodol.*, vol. 96, pp. 26–45, Feb. 2017.

[16] M. Yildirimoglu, M. Ramezani, and N. Geroliminis, "Equilibrium analysis and route guidance in large-scale networks with MFD dynamics," *Transp. Res. C, Emerg. Technol.*, vol. 59, pp. 404–420, Oct. 2015.

[17] N. Zheng and N. Geroliminis, "Modeling and optimization of multimodal urban networks with limited parking and dynamic pricing," *Transp. Res. B, Methodol.*, vol. 83, pp. 36–58, Jan. 2016.

[18] M. Amirgholy, M. Shahabi, and H. O. Gao, "Optimal design of sustainable transit systems in congested urban networks: A macroscopic approach," *Transp. Res. E, Logistics Transp. Rev.*, vol. 103, pp. 261–285, Jul. 2017.

[19] M. Ramezani and M. Nourinejad, "Dynamic modeling and control of taxi services in large-scale urban networks: A macroscopic approach," *Transp. Res. C, Emerg. Technol.*, vol. 23, pp. 41–60, Jan. 2017.

[20] M. Keyvan-Ekbatani, A. Kouvelas, I. Papamichail, and M. Papageorgiou, "Exploiting the fundamental diagram of urban networks for feedback-based gating," *Transp. Res. B, Methodol.*, vol. 46, no. 10, pp. 1393–1403, Dec. 2012.

[21] K. Aboudolas and N. Geroliminis, "Perimeter and boundary flow control in multi-reservoir heterogeneous networks," *Transp. Res. B, Methodol.*, vol. 55, pp. 265–281, Sep. 2013.

[22] M. Keyvan-Ekbatani, M. Yildirimoglu, N. Geroliminis, and M. Papageorgiou, "Multiple concentric gating traffic control in large-scale urban networks," *IEEE Trans. Intell. Transp. Syst.*, vol. 16, no. 4, pp. 2141–2154, Aug. 2015.

[23] J. Haddad and A. Shraiber, "Robust perimeter control design for an urban region," *Transp. Res. B, Methodol.*, vol. 68, pp. 315–332, Oct. 2014.

[24] J. Haddad, "Robust constrained control of uncertain macroscopic fundamental diagram networks," *Transp. Res. C, Emerg. Technol.*, vol. 59, pp. 323–339, Oct. 2015.

[25] L. Leclercq, N. Chiabaut, and B. Trinquier, "Macroscopic fundamental diagrams: A cross-comparison of estimation methods," *Transp. Res. B, Methodol.*, vol. 62, pp. 1–12, Apr. 2014.

[26] J. Du, H. Rakha, and V. V. Gayah, "Deriving macroscopic fundamental diagrams from probe data: Issues and proposed solutions," *Transp. Res. C, Emerg. Technol.*, vol. 66, pp. 136–149, May 2016.

[27] L. Ambühl and M. Menendez, "Data fusion algorithm for macroscopic fundamental diagram estimation," *Transp. Res. C, Emerg. Technol.*, vol. 71, pp. 184–197, Oct. 2016.

[28] A. Zockaie, M. Saberi, and R. Saedi, "A resource allocation problem to estimate network fundamental diagram in heterogeneous networks: Optimal locating of fixed measurement points and sampling of probe trajectories," *Transp. Res. C, Emerg. Technol.*, vol. 86, pp. 245–262, Jan. 2018.

[29] J. Haddad, "Optimal perimeter control synthesis for two urban regions with aggregate boundary queue dynamics," *Transp. Res. B, Methodol.*, vol. 96, pp. 1–25, Feb. 2017.

[30] J. Haddad, "Optimal coupled and decoupled perimeter control in one-region cities," *Control Eng. Pract.*, vol. 61, pp. 134–148, Apr. 2017.

[31] D. S. Naidu, *Optimal Control Systems*. Boca Raton, FL, USA: CRC Press, 2002.

[32] D. C. Gazis, "Optimum control of a system of oversaturated intersections," *Oper. Res.*, vol. 12, no. 6, pp. 815–831, 1964.

[33] J. C. Mason and D. C. Handscomb, *Chebyshev Polynomials*. Boca Raton, FL, USA: CRC Press, 2002.

[34] T. Zhao, C. Li, Z. Zang, and Y. Wu, "Chebyshev–Legendre pseudo-spectral method for the generalised burgers–Fisher equation," *Appl. Math. Model.*, vol. 36, no. 3, pp. 1046–1056, 2012.

[35] C. Canuto, M. Y. Hussaini, A. Quarteroni, and T. A. Zang, Jr., *Spectral Methods in Fluid Dynamics*. Berlin, Germany: Springer-Verlag, 2012.

[36] D. E. Kirk, *Optimal Control Theory: An Introduction*. North Chelmsford, MA, USA: Courier Corporation, 2012.

[37] R. F. Hartl, S. P. Sethi, and V. G. Raymond, "A survey of the maximum principles for optimal control problems with state constraints," *SIAM Rev.*, vol. 37, no. 2, pp. 181–218, 1995.

[38] S. P. Sethi and G. L. Thompson, *Optimal Control Theory.* New York, NY, USA: Springer, 2000.

[39] R. Vinter, *Optimal Control*. Basel, Switzerland: Springer-Birkhäuser, 2010.

[40] C. F. Daganzo, "Urban gridlock: Macroscopic modeling and mitigation approaches," *Transp. Res. B, Methodol.*, vol. 41, no. 1, pp. 49–62, 2007.

[41] M. R. Osborne, "On shooting methods for boundary value problems," *J. Math. Anal. Appl.*, vol. 27, no. 2, pp. 417–433, 1969.

[42] Z. Nikooeinejad, A. Delavarkhalafi, and M. Heydari, "A numerical solution of open-loop Nash equilibrium in nonlinear differential games based on Chebyshev pseudospectral method," *J. Comput. Appl. Math.*, vol. 300, pp. 369–384, Jul. 2016.

[43] J. P. Boyd, *Chebyshev & Fourier Spectral Methods*. North Chelmsford, MA, USA: Courier Corporation, 2001.

[44] B. Fornberg, *A Practical Guide to Pseudospectral Methods*, vol. 1. Cambridge, U.K.: Cambridge Univ. Press, 1998.

Ali Aalipour received the B.Sc. degree in electrical engineering (control systems) from the K. N. Toosi University of Technology, Tehran, Iran, in 2014. He is currently pursuing the M.Sc. degree with the Smart Networks Laboratory, School of Electrical and Computer Engineering, University of Tehran, Iran, under the supervision of Dr. H. Kebriaei and Dr. M. Ramezani. His research interests include optimization and stochastic control, nonlinear robust control, and traffic flow control.

Hamed Kebriaei (M'14–SM'18) received the B.Sc. degree in electrical engineering from the University of Tehran, Tehran, Iran, in 2005, the M.Sc. degree in electrical engineering from Tarbiat Modares University, Tehran, in 2007, and the Ph.D. degree in control systems from the University of Tehran in 2010. From 2014 to 2015, he was a Visiting Professor with the Department of Automatic Control, University of Sannio, Italy. He is currently an Assistant Professor of control systems with the School of Electrical and Computer Engineering, University of Tehran. His research interests include game theory, optimization, and stochastic control with applications in wireless communication and networking and smart grids.

Mohsen Ramezani (S'09–M'10) received the B.Sc. and M.Sc. degrees in electrical engineering (control systems) from the University of Tehran, Tehran, Iran, in 2008 and 2010, respectively, and the Ph.D. degree in transportation from the École Polytechnique Fédérale de Lausanne, Switzerland, in 2014. He is currently a Lecturer (Assistant Professor) with the School of Civil Engineering, The University of Sydney. His research interests include intelligent transportation systems, traffic control, and traffic flow operations. He was a recipient of the 2015 IEEE Intelligent Transportation Systems Society 1st Prize Best Ph.D. Dissertation.